Amyloid-β Peptide Assembly: A Critical Step in Fibrillogenesis and Membrane Disruption

Christopher M. Yip* and JoAnne McLaurin†

*Institute for Biomaterials and Biomedical Engineering and Centre for Studies in Molecular Imaging, †Centre for Research in Neurodegenerative Diseases, *Departments of Chemical Engineering and Applied Chemistry, *Biochemistry, and †Laboratory Medicine and Pathobiology, University of Toronto, Toronto, Ontario M5S 3G9 Canada

ABSTRACT Identifying the mechanisms responsible for the assembly of proteins into higher-order structures is fundamental to structural biology and understanding specific disease pathways. The amyloid-β (Aβ) peptide is illustrative in this regard as fibrillar deposits of Aβ are characteristic of Alzheimer's disease. Because Aβ includes portions of the extracellular and transmembrane domains of the amyloid precursor protein, it is crucial to understand how this peptide interacts with cell membranes and specifically the role of membrane structure and composition on Aβ assembly and cytotoxicity. We describe the results of a combined circular dichroism spectroscopy, electron microscopy, and in situ tapping mode atomic force microscopy (TMAFM) study of the interaction of soluble monomeric Aβ with planar bilayers of total brain lipid extract. In situ extended-duration TMAFM provided evidence of membrane disruption via fibril growth of initially monomeric Aβ1–40 peptide within the total brain lipid bilayers. In contrast, the truncated Aβ1–28 peptide, which lacks the anchoring transmembrane domain found in Aβ1–40, self-associates within the lipid headgroups but does not undergo fibrillogenesis. These observations suggest that the fibrillogenic properties of Aβ peptide are in part a consequence of membrane composition, peptide sequence, and mode of assembly within the membrane.

INTRODUCTION

Amyloid-β (Aβ) peptide is derived by proteolytic processing of the extracellular and transmembrane regions of the membrane-anchored amyloid precursor protein (APP) and has been causally linked with the formation of diffuse and senile plaques (Esch et al., 1990; Haass et al., 1992; Masters et al., 1985; Roher et al., 1986). The overproduction and deposition of Aβ are characteristics of Alzheimer's disease, Down's syndrome, and hereditary cerebral hemorrhagic disease, HCWA-D (Dutch type; Cai et al., 1993; Citron et al., 1994; Iwatsubo et al., 1995; Suzuki et al., 1994). In vivo, Aβ is released as a monomeric peptide (Esch et al., 1990; Haass et al., 1992), but during normal aging or as a result of a disease process, Aβ self-associates into fibers that precipitate as plaques in the brain parenchyma. This process is enhanced by increased peptide concentrations, altered pH, and non-Aβ nucleation seeds. In vitro studies have demonstrated that synthetic Aβ can assemble spontaneously into β-sheet-containing fibrils (Halverson et al., 1990; Kirschner et al., 1986; Lomakin et al., 1996; Walsh et al., 1997), that fibrillar Aβ can induce neuritic dystrophy (Lorenzo and Yankner, 1994; Pike et al., 1993; Simmons et al., 1993; Soto et al., 1995), and that Aβ-induced cellular degeneration occurs due to stimulation of inappropriate cell signals (Behl et al., 1994; Giulian et al., 1996; Mattson et al., 1997; Paradis et al., 1996). These observations suggest that defining the role of Aβ in mitigating specific disease pathways requires careful characterization of both the biological activity and the active conformation of the protein.

Because Aβ bears a portion of the APP transmembrane domain, it has been proposed that it may modulate membrane function by altering the physicochemical properties of various membrane constituents. These perturbations may include disruption of leaflet structure, an increase in bilayer curvature, or formation of membrane channels (Arispe et al., 1993; Choo-Smith and Surewicz, 1997; Mason et al., 1996, 1999; McLaurin and Chakrabartty, 1996; McLaurin et al., 1997, 1998; Mirzabekov et al., 1994; Pillot et al., 1996, 1997; Terzi et al., 1994, 1995). Although recent studies have demonstrated that lipids, and in particular acidic phospholipids, can induce a conformational transition in Aβ from random to β-structure, a process that enhances fibril formation and initiates destabilization of the associated membrane structure, the fundamental mechanisms associated with these events remain unknown (Arispe et al., 1993; Choo-Smith and Surewicz, 1997; McLaurin and Chakrabartty, 1996, 1997; McLaurin et al., 1997, 1998; Terzi et al., 1994, 1995).

These questions prompted us to investigate the membranolytic action of Aβ peptides on planar bilayers of total brain lipid extract by circular dichroism (CD) spectroscopy, electron microscopy, and in situ solution tapping mode atomic force microscopy (TFAFM). This latter technique has proven to be a powerful approach for deciphering biomolecular assembly and protein structure under near-native conditions (Hansma et al., 1994; Karrasch et al., 1994; Möller et al., 1999), including Aβ-fibrillogenesis (Blackley et al., 1999; Harper et al., 1997; Kowalewski and Holtzman,

Received for publication 15 May 2000 and in final form 15 December 2000.

Address reprint requests to Dr. JoAnne McLaurin, Centre for Research in Neurodegenerative Diseases, Tanz Neuroscience Building, 6 Queen's Park Crescent West, Toronto, Ontario, Canada M5S 3H2. Tel.: 416-978-1035; Fax: 416-978-1878; E-mail: j.mclaurin@utoronto.ca.

0006-3495/01/03/1359/13 $2.00

1999; Oda et al., 1995; Roher et al., 1993, 1996; Stine et al., 1996). We have applied TMAFM to study protein assembly into the crystalline solid state (Yip and Ward, 1996; Yip et al., 1998a,b, 2000), role of chemical chaperones in modulating Aβ aggregation (Yang et al., 1999), and the oriented association of proteins at lipid interfaces (Plaskos and Yip, 2000).

The present studies provide evidence that the mechanism of Aβ−induced membrane disruption is strongly dependent on both lipid composition and peptide structure and conformation. Our in situ observation by TMAFM that Aβ fibril formation occurs in association with the lipid bilayer only in the presence of acidic lipids and only when the transmembrane domain of Aβ is present suggests that membrane anchoring is important for fibrillogenesis whereas amorphous aggregation is favored in the absence of the acidic lipid and/or the anchoring Aβ29−40 transmembrane domain. These results illustrate that peptide structure and sequence and membrane composition dramatically influence protein assembly (or misassembly) at membrane interfaces.

MATERIALS AND METHODS

Peptides

Aβ1−28 and Aβ1−40 were synthesized by solid-phase Fmoc chemistry by the Hospital for Sick Children's Biotechnology Centre (Toronto, Ontario, Canada). Peptides were purified by reverse-phase HPLC on a C18 μbondapak column. Peptides were initially dissolved in 0.5 ml of 100% trifluoroacetic acid (Aldrich Chemicals, Milwakee, WI) to ensure that the peptide remained monomeric and free of fibril seeds, diluted in distilled H_2O, and immediately lyophilized (Jao et al., 1997). Peptides were then dissolved at 1 mg/ml in 40% trifluoroethanol (TFE, Aldrich Chemicals) in H_2O and stored at −20°C until use. Alternatively, the lyophilized peptides were dissolved at 10 mg/ml in PBS.

Lipids

Dimyristylphosphatidylcholine (DMPC) and total brain lipid extract were purchased from Avanti Lipids (Alabaster, AL). To prepare the bilayer suspensions, the lipids were dried under a stream of nitrogen, lyophilized, and resuspended in PBS (pH 7.4) at a concentration of 1 mg/ml. Lipid suspensions were carried through five cycles of freeze-thaw in an acetone-solid CO_2 bath, which forms both bilayer and multilayer lipid sheets. The lipid suspensions were then bath sonicated for 15–20 min to ensure formation of vesicles.

Circular dichroism spectroscopy

CD spectra were recorded on an Aviv CD spectrometer model 62DS (Lakewood, NJ) at 25°C. Spectra were obtained from 200–260 nm, with a 0.5-nm step, 1-nm bandwidth and 10-s collection time per step. The effects of the lipids on peptide conformation were determined by adding an aliquot of stock peptide solutions to lipid suspended in PBS (pH 7.4) at a 1:20 ratio (by weight). Final peptide concentration was 10 μM. CD spectra were examined immediately after addition of Aβ and over a 24-h time course. The contribution of lipids to the CD signal was removed by subtracting the lipid-only spectra (McLaurin and Chakrabartty, 1996). Spectra were deconvoluted using Prosce (Yang et al., 1986).

Electron microscopy

Aβ1−40 was incubated in the presence and absence of total brain lipid extract bilayers at a final peptide concentration of 0.1 mg/ml. The Aβ-to-lipid ratio was maintained at 1:20 (by weight) matching the solutions sampled by CD. Preformed Aβ1−40 fibrils were prepared by incubating a 10 mg/ml solution of Aβ1−40 for 3 days at room temperature. For negative-stain electron microscopy, carbon-coated pioloform grids were floated on aqueous solutions of peptides. After grids were blotted and air-dried, the samples were stained with 1% (w/v) phosphotungstic acid. The peptide assemblies were observed in a Hitachi 7000 electron microscope operated at 75 V.

Atomic force microscopy

Solution TMAFM images were acquired on a Digital Instruments Nanoscope IIIA MultiMode scanning probe microscope (Digital Instruments, Santa Barbara, CA) using 120-μm oxide-sharpened silicon nitride V-shaped cantilevers installed in combination contact/tapping mode liquid flow cell. The AFM images were acquired using the E scanning head, which has a maximum lateral scan area of 14.6 μm × 14.6 μm. All imaging was performed at tip scan rates from 1.25 to 2 Hz, using cantilever drive frequencies of ~8.9 kHz (Yip et al., 1996). All images were captured as 512 × 512 pixel images and were low-pass filtered. Feature size and volumes were calculated using the Digital Instruments Nanoscope software (version 4.21) and shareware image analysis program National Institutes of Health-Image (version 1.62). Lateral calibration of the AFM piezoscanner was effected by resolving the crystallographic lattice of the basal plane of freshly cleaved mica and graphite whereas the vertical calibration was performed by measuring mica and graphite step heights in fluid. In situ TMAFM experiments were performed by sequential addition of the solutions to the AFM fluid cell. Planar bilayers were formed by directly injecting ~500 μl of the 1 mg/ml lipid suspension into the AFM fluid cell, previously sealed against a piece of freshly cleaved mica and allowing the vesicles to fuse in situ (Plaskos and Yip, 2000). The cell was flushed with neat buffer and reference TMAFM height and phase images acquired in PBS (pH 7.4) to confirm formation of stable lipid bilayers. Approximately 500 μl of a 0.1 mg/ml PBS solution of the peptide of interest (Aβ1−40 or Aβ1–28) was injected directly into the AFM cell and imaging initiated 30 min after Aβ addition.

RESULTS

Secondary structure of Aβ in the presence of lipid bilayers

Recognizing that Aβ-fibrillogenesis (Halverson et al., 1990; Lomakin et al., 1996; Walsh et al., 1997) and Aβ-lipid interactions (McLaurin and Chakrabartty, 1996) are dependent on initial Aβ structure, the Aβ1−40 and Aβ1–28 peptides were dissolved in 100% trifluoroacetic acid and immediately lyophilized to ensure that they were monomeric, in a random conformation, and free of fibril seeds (Jao et al., 1997). Secondary structure of Aβ1−40 and Aβ1–28 in the presence and absence of lipid bilayers was determined using CD spectroscopy (Fig. 1). Total brain lipid extract is ideally suited for these studies as it provides a physiologically relevant ratio of membrane components, including acidic and neutral phospholipids, gangliosides, cholesterol, sphingolipids, and isoprenoids. For our control experiments, planar bilayers of the zwitterionic lipid DMPC

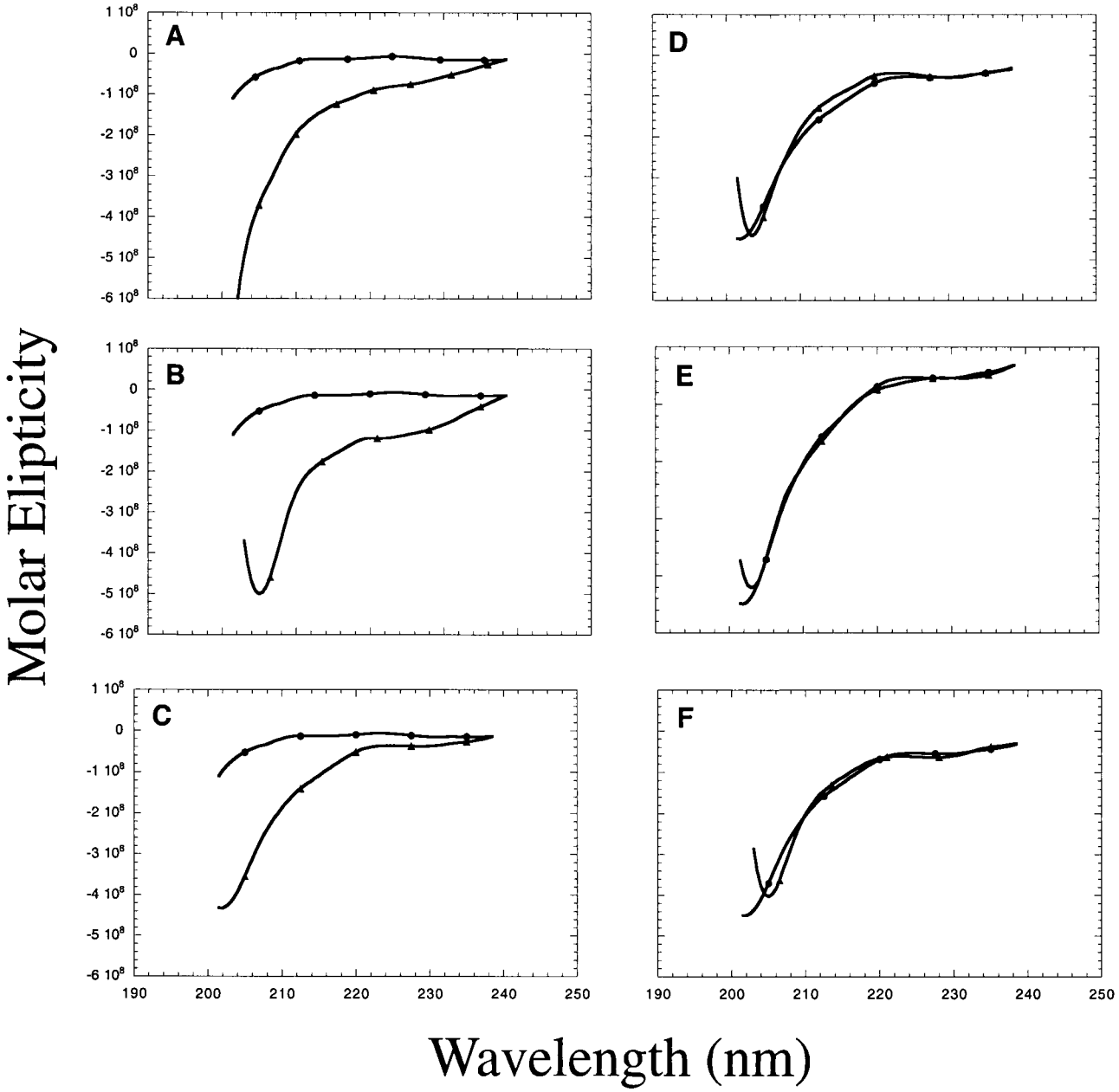

FIGURE 1 Circular dichroism spectra of Aβ1–40 and Aβ1–28 in the absence and presence of lipid. Differences in the CD spectra of Aβ1–40 obtained in PBS pH 7.4 (*A*), and in the presence of total brain lipid extract (*B*) and DMPC (*C*) at a 1:20 peptide-to-lipid ratio with a final peptide concentration of 10 μM, demonstrate that upon initial mixing (●), Aβ1–40 is random structured in the presence and absence of all lipids. Over time, however, Aβ1–40 undergoes a conformational transition as evidenced by the altered CD spectra. In contrast, Aβ1–28 in PBS (*D*) and in the presence of total brain lipid extract (*E*) and DMPC (*F*) at a 1:20 peptide-to-lipid ratio with a final peptide concentration of 10 μM were superimposable. The CD spectra were collected on a 24-h time period with representative curves at 24 h (▲) depicted.

were used as the interactions of Aβ with this lipid have been reported previously in the literature (Arispe et al., 1993; McLaurin and Chakrabartty, 1996, 1997; McLaurin et al., 1997, 1998; Terzi et al., 1994, 1995).

Time-course CD spectroscopy performed over a 24-h period on Aβ1–40 in PBS pH 7.4 revealed that the initially randomly structured peptide, when mixed at a 1:20 peptide-to-lipid ratio to a final peptide concentration of 10 μM underwent a partial conformational change in the presence of total brain lipid but remained random in the presence of DMPC vesicles (Fig. 1, *A–C*). In the presence of total brain lipid vesicles, the time-course CD spectra revealed the gradual development of a spectral change indicative of both random and β-structure in the Aβ1–40 peptide (Fig. 1 *B*).

Deconvolution of CD spectra indicates a 77% random and 21% β-structure in the presence of total brain lipid extract in comparison with Aβ40 alone, 82% random and 15% β-structure. Because CD represents an average of all species present in solution, it is not possible to discern a single population associated with lipid vesicles. CD measurement accuracy is limited by the methodology used to determine peptide concentrations. Previous studies have demonstrated that amino acid analysis and ninhydrin techniques for peptide quantitation typically lead to an underestimation of peptide concentration by ~10%, which leads to 10–20% higher mean ellipticity values (Marquess et al., 1989). Alternatively, the use of tyrosine absorbance in trifluoroethanol, as is used routinely in our laboratory, is accurate within 2%, representing a more accurate and more precise method (Marquess et al., 1989). It should also be noted that β-structure is inherently underestimated by current deconvolution programs. Nevertheless, our CD data are consistent with the random structure Aβ1–40 peptide undergoing a β-structure transformation upon binding to the total brain lipid vesicles. We cannot rule out the possibility that random structured Aβ1–40 peptides are in fact associated with the lipid (as well as being in solution); however, previous studies have demonstrated that acidic lipids can induce a β-structural transition (McLaurin and Chakrabartty, 1996, 1997; McLaurin et al., 1997, 1998; Terzi et al., 1994, 1995). Control experiments performed with the zwitterionic lipid DMPC revealed that the Aβ1–40 peptide retains mostly a random conformation, 88%, over a 24-h time period (Fig. 1 *C*). Time-course CD studies performed with the N-terminal peptide Aβ1–28 revealed that its predominantly random structure was unchanged in the presence of total brain lipid extract and DMPC (Fig. 1, *D–F*). CD spectra at 24 h were superimposable on the spectra collected within 30 s of mixing Aβ1–28 with lipid vesicles.

Structural details of Aβ-lipid interactions

The relationship between the spectroscopically observed conformational transition of Aβ1–40 in the presence of total brain lipid extracts, fibril formation, and membrane disruption is largely unknown. Although various models of Aβ fibril formation have been proposed, they all agree that the β-sheet regions are defined by the hydrophobic internal residues 17–21 and C-terminal residues 29–40/42. Fibrillogenesis is viewed as a two-step process involving a slow lag phase associated with the thermodynamic barrier to seed formation and fibril nucleation and a more rapid fibril growth and aggregation stage. These phases are known to be mediated by various factors including peptide concentration, changes in the Aβ peptide primary sequence, pH, and interactions with other elements that stimulate Aβ aggregation (reviewed in McLaurin et al., 2000).

Traditionally, electron microscopy has been used to evaluate Aβ fibrillar structures and peptide-lipid interactions. However, the sample preparation requirements of negative-stain electron microscopy are problematic due to issues related to sample drying and staining procedures. These limitations restrict EM interpretation to the physical characteristics (shape/size) of the fibrils and rule out real-time interpretation of aggregation kinetics. With these limitations in mind, negative-stain electron microscopy revealed mature Aβ1–40 fibers extending along the peripheral surface of total brain lipid extract vesicles after a 3-day incubation (Fig. 2 *A*). However, these images are acquired ex situ and thus can provide only indirect evidence of association between the Aβ1–40 fibers and intact vesicles. Therefore, to study the real-time kinetics of Aβ-lipid interactions, in situ solution TMAFM was used.

In intermittent-contact, or tapping-mode, AFM, the scanning tip is vertically oscillated during scanning, which reduces frictional loads on the sample and thus the potential for sample distortion. Although TMAFM height imaging provides details on surface topography, phase imaging measures the relative phase shift between the applied and detected tip oscillation during TMAFM imaging and thus can provide information regarding intrinsic local surface modulus and viscoelasticity (Winkler et al., 1996). In fluid, the observed phase shift reflects differences in the amount of energy dissipated during tip contact with the surface and may correlate with specific adhesive interactions between the tip and surface, with the degree of phase shift increasing with increasing adhesion and energy dissipation (Brandsch et al., 1997; Cleveland et al., 1998; Czajkowsky et al., 1998; Noy et al., 1998). For our purposes, this mode of imaging can distinguish between lipid islands and aggregated protein patches on top of the lipid bilayers and has the potential for identifying structurally dissimilar domains within a lipid bilayer that may not be detectable by topographical contrast.

In situ formation of lipid bilayers within the AFM fluid cell was accomplished by continuously imaging the fusion of a 1 mg/ml lipid vesicle suspension onto the mica surface (Brian and McConnell, 1984). Previous studies have shown that supported bilayers are typically separated from the solid support by a thin buffer film and retain many of the properties of free membranes, including lateral fluidity (Bayerl and Bloom, 1991; Salafsky et al., 1996; Groves et al., 1997). AFM imaging was used to monitor the deposition of lipid vesicles from solution to the mica surface and their subsequent spreading and lateral fusion into molecularly flat bilayers populated by small amorphous globules and disc-shaped islands. We note that bilayers were not used unless they were found to be essentially defect-free (i.e., no exposure of the underlying mica) over randomly selected >50-μm^2 scan areas (Fig. 3 *A*).

In situ TMAFM revealed Aβ1–40 protruding ~10 Å above the smooth ~40-Å-thick total brain lipid extract bilayers, ~30 min after the addition of 0.1 mg/ml Aβ1–40 (Fig. 3 *B*). We were able to distinguish the Aβ1–40 molecules from the lipid globules and islands by both height and

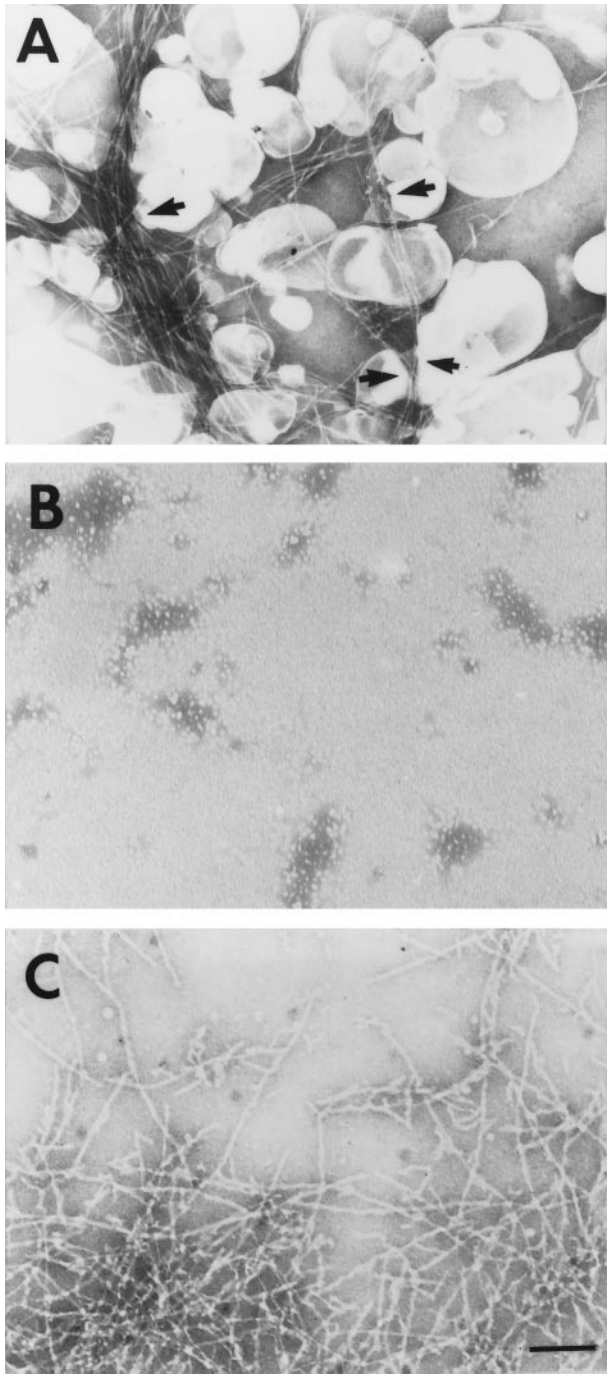

FIGURE 2 Negative-stain electron microscopy of Aβ1−40 in the presence and absence of lipids. (*A*) Preparations of Aβ1–40, in the presence of total brain lipid extract, give rise to fibers that grow along the surface of vesicles (*arrowheads* delineate lipid edges) with some apparent aggregation. (*B* and *C*) Aβ1–40 incubation for 24 h in PBS at 0.1 mg/ml did not cause fibril formation (*B*) whereas preincubation of Aβ1–40 for 3 days at 10 mg/ml resulted in formation of long mature fibers (*C*). Bar, 100 nm.

phase imaging as the lipid islands and globules typically extended ~35–40 Å above the underlying ~40-Å-thick bilayer whereas the phase contrast of the lipid globules and islands was intermediate to that of the peptide and the supporting bilayer. The lipid islands were also morphologically distinguishable from the Aβ molecules. We attribute the variations in phase contrast to local differences in the energy dissipated by these structures as they interact with the oscillating AFM tip (Winkler et al., 1996, Brandsch et al., 1997; Cleveland et al., 1998; Czajkowsky et al., 1998; Noy et al., 1998).

The physiological structure of Aβ has yet to be determined as its tendency to aggregate and polymerize has limited the use of classical techniques such as crystallography. Previous in situ AFM imaging has determined that two-stranded β-sheet structured Aβ1−42 has an approximate volume of 10,000 Å (Yang et al., 1999) and Aβ40 has dimensions of 1–2 nm in diameter (Walsh et al., 1997). Alternatively, NMR studies of Aβ1–40 and Aβ1–28 peptides have determined that the Aβ1–28 domain is ~35 Å in length whereas the full 40-residue peptide has a length of ~48 Å (Sticht et al., 1995; Talafous et al., 1994). Using these two divergent techniques as an indicator of size, the extent of Aβ1–40 exposure as determined by TMAFM suggests partial insertion of the peptide into the bilayer, likely through the 29–40 hydrophobic domain. At 3 h after peptide addition, small Aβ fibers were barely visible on the surface of or within lipid headgroups using TMAFM height imaging (Fig. 4 *A*). To elucidate the presence of Aβ fibrils, TMAFM phase images were examined. The use of phase imaging to differentiate lipid and fibers that appear to be in the same plane topographically is based on local surface differences in viscoelasticity and differential adhesive interactions between the lipid and peptide with the tip. Although not easily resolvable by topographical contrast, phase imaging provided evidence of Aβ1–40 fibrils growing within the bilayer (Fig. 4 *B*). Examination of the height and phase images revealed the presence of small fibers not associated with disrupted lipid regions. This indicates that the lipid headgroups can initially accommodate fibril growth. Larger fibers could be detected and appear adjacent to the initiation of small lipid disruptions. These images represent an intermediate phase in Aβ fibrillogenesis (Fig. 4).

The gradual growth of 120–180-Å-wide Aβ1–40 fibrils in the bilayer was revealed by in situ TMAFM and phase imaging performed over 24 h (Fig. 3 *C*). The fibrils are in the plane of and extend parallel to the bilayer surface, suggesting that fibril nucleation and growth occur within the lipid headgroups (Fig. 3 *C*, *inset*). We cannot discount lateral diffusion of Aβ1–40 through the bilayer although we did not observe this process on the time scale of the TMAFM imaging (minutes). The absence of Aβ1–40 aggregates indicate that, for total brain lipid extract, Aβ1–40 interaction with lipid domains facilitates formation of the fibril. The lack of Aβ aggregates suggests that off-pathway intermediates, reported for solution-grown fibrils (Huang et al., 2000), are not formed in the presence of total brain lipid extract bilayers.

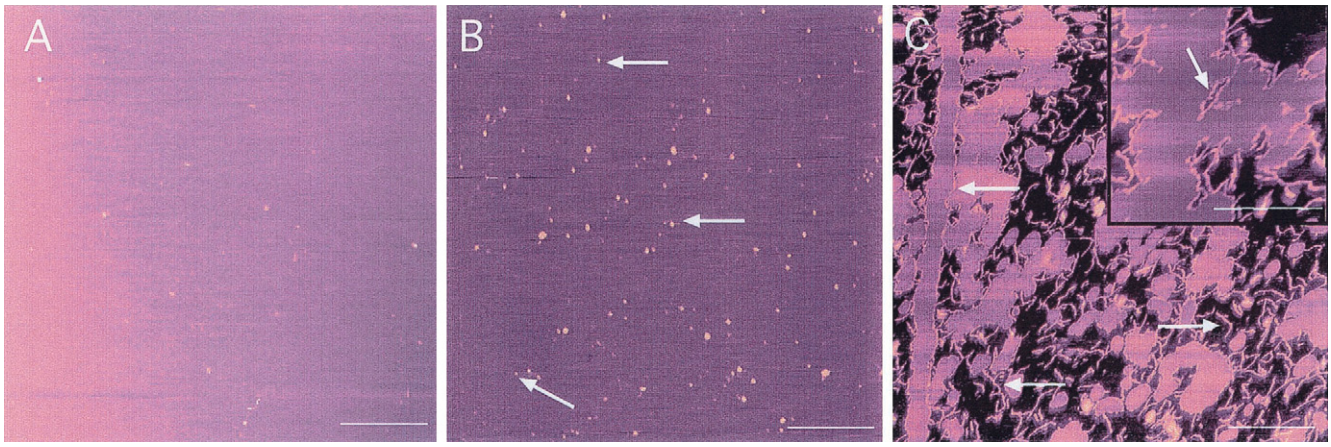

FIGURE 3 In situ TMAFM height images acquired in PBS of the interaction between Aβ1–40 and total brain lipid extract bilayers. (*A*) Intact defect-free total brain lipid bilayers before the addition of Aβ illustrate smooth bilayer surfaces (A). (*B*) Aβ1–40 molecules were found partially inserted into the total brain lipid bilayer. (*C*) Fibril growth initiates at these sites and fibrils grow through the bilayer resulting in excision of large membrane patches; image acquired 15 h after *B*. Inset image in *C* reveals that the fibrils are forming within the bilayer and not only associated with membrane edges and mica surface. (*A–C*) Scale bar, 2 μm; (*inset*) scale bar, 1 μm. All images are height encoded by color with the lower underlying mica substrate shown in black and the lighter colors representing taller features.

In situ TMAFM imaging revealed extensive destabilization of the total brain lipid extract bilayer after Aβ1–40 fibril growth had initiated (Fig. 3 *C*). We found no evidence of bilayer defects before the introduction of monomeric Aβ1–40 (Fig. 3 *A*), nor did we observe any incidence of tip-induced bilayer damage, either before or after fibril formation. In the disrupted membrane regions, Aβ1–40 fibrils were associated with bilayer edges and extended across the exposed mica substrate (Fig. 3 *C*). Both membrane-bound and exposed fibrils were branched, and the degree of branching appeared to be greater than that reported for solution-grown fibrils (Blackley et al., 1999; Harper et al., 1997; Kowalewski and Holtzman, 1999; Oda et al., 1995; Roher et al., 1996; Stine et al., 1996). This

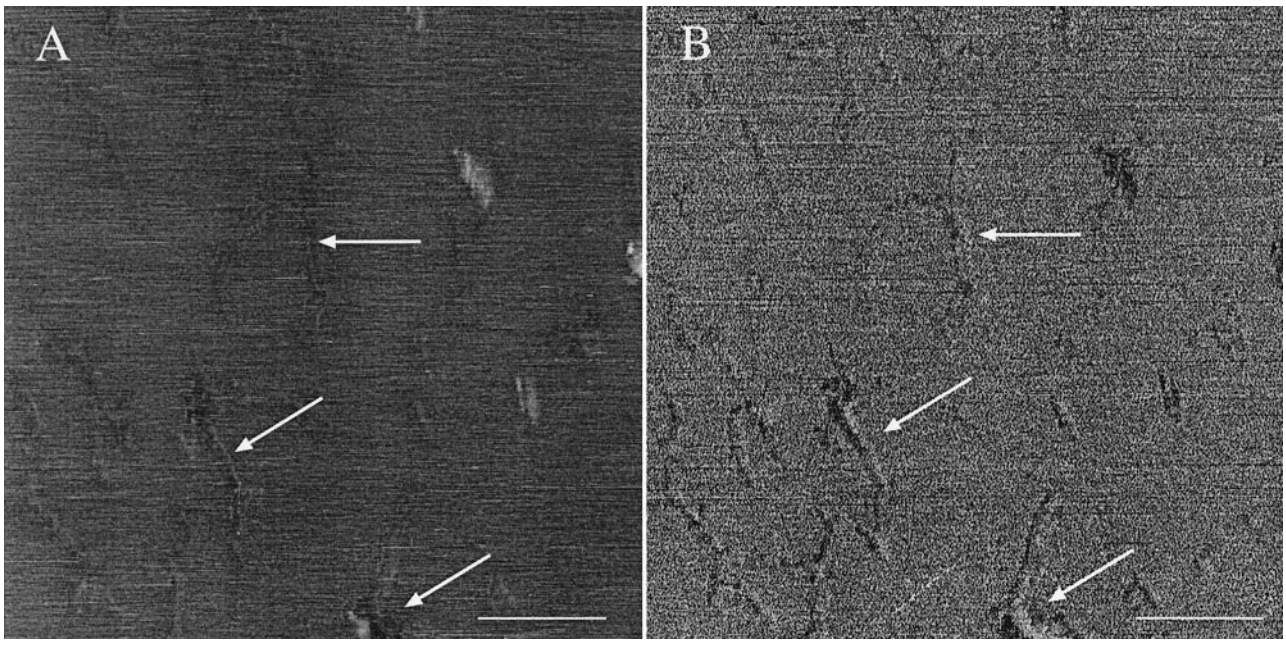

FIGURE 4 In situ TMAFM height images acquired in PBS of the interaction between Aβ1–40 and total brain lipid extract bilayers. Height images of bilayers 3 h after the addition of Aβ demonstrate barely discernable small fibrils (*A*), whereas the corresponding phase image distinguishes the presence of Aβ fibrils within the lipid (*B*, *arrows*). Comparison of the two data sets demonstrates small Aβ fibrils in the bilayer in the absence and presence of small bilayer defects. Scale bar; 200 nm.

increased branching may result from growing fibrils encountering membrane patches that are energetically impermeable to fiber growth, either due to specific lipid composition or tighter packing of the lipid headgroups. To rule out tip interference over the time course of our experiment, randomly chosen scan areas were examined. Although massive membrane disruption was detected after 15 h, less disrupted areas also were present (Fig. 5 *A*). High-resolution phase imaging of the less disrupted areas revealed small Aβ fibers within the intact bilayer headgroups in regions that were not associated with bilayer defects (Fig. 5 *B*).

We considered the possibility that the fibrils we observed were a consequence of solution fibril growth and deposition to the bilayer surface. To address this concern, the same 0.1 mg/ml Aβ1–40 solution used in the bilayer studies was left to incubate at room temperature while we conducted our bilayer studies. In situ TMAFM imaging and negative-stain electron microscopy performed on aliquots of this solution after 24 h did not reveal any fibrillar aggregates although small peptide monomers or oligomers were found (Figs. 2 *B* and 5 *C*). These observations would suggest that fibril nucleation is facilitated by the lipid bilayer and that the structures observed by in situ TMAFM are in fact not due to fibril formation in the surrounding fluid.

We propose that by displacing lipid from the bilayer as it forms, the growing fibril weakens the stabilizing lipid-lipid lateral interactions within the bilayer and initiates the release of small bilayer patches. We did on occasion find small fibrils that were not associated with a particular bilayer edge or that appeared to extend away from a bilayer island (data not shown). We propose that these are fibrils left behind once the membrane patch has been destabilized and released into the surrounding buffer.

Lipid specificity of Aβ interactions

To investigate the role of lipid composition in Aβ-induced membrane disruption, planar DMPC bilayers were employed as model substrates. As described above, AFM imaging was used to monitor the fusion of lipid vesicles onto the mica and subsequent spreading to form an intact bilayer. Bilayers were not used unless they were found to be essentially defect-free over randomly selected scan areas. In situ TMAFM imaging revealed Aβ1–40 extending ~12–25 Å above the DMPC bilayer surface (Fig. 6 *A*). Aβ1–40 was typically located adjacent to small ~20-Å-wide holes, suggesting that the insertion process facilitated local disruption of the bilayer. These holes extend through the bilayer to expose the underlying mica substrate. TMAFM imaging performed over a 15-h time period revealed the gradual expansion of irregular patches of Aβ1–40 aggregates throughout the DMPC bilayer (Fig. 6 *B*). Initially, we found no evidence of the Aβ1–40 peptide on the exposed mica surfaces or within the bilayer holes, which suggests that the peptide prefers to self-associate or associate with the zwitterionic lipid. In these patches, the Aβ1–40 aggregates protrude up to 100 Å above the bilayer surface, not only indicating that Aβ1–40 interacts with the bilayer but also confirming self-association (Fig. 6 *B*). In contrast to our total brain lipid extract studies, only globular aggregate masses of Aβ1–40 were found in the DMPC bilayers; no fibrils formed over a 24-h time period. These results suggest that the critical step in membrane destabilization is Aβ1–40 self-assembly into fibers and aggregates on the bilayer surface.

This model was examined by studying the interaction of preformed Aβ1–40 fibrils or aggregates with planar bilayers (Fig. 6). Negative-stain EM demonstrated that fibrils

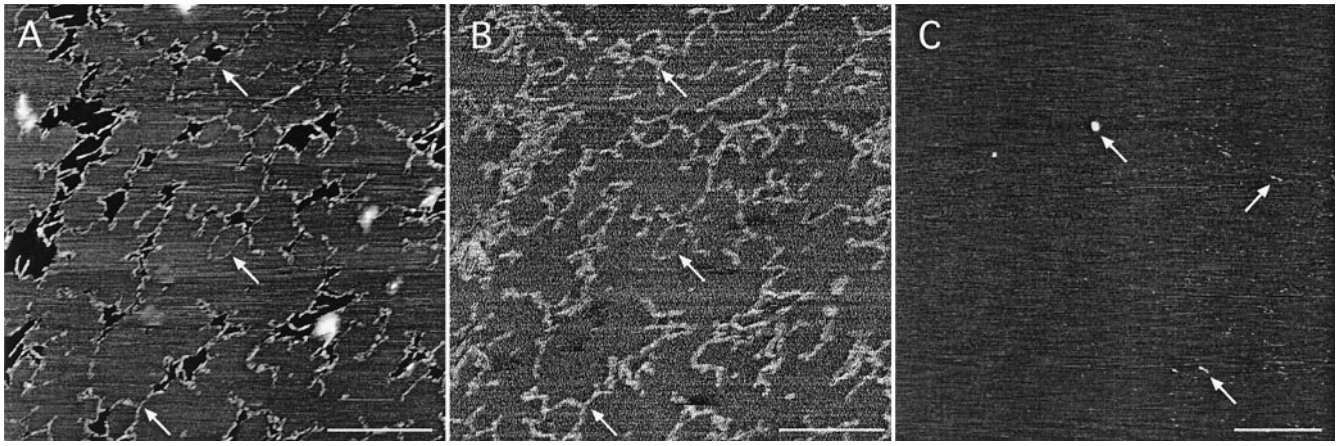

FIGURE 5 In situ TMAFM height and phase imaging of Aβ1–40 interactions with total brain lipid planar bilayers. (*A*) Height images reveal Aβ1–40 fibrils growing through the bilayer, which results in membrane perturbations. (*B*) The use of phase imaging reveals Aβ fibrils growing within the bilayer not associated with membrane disruptions that do not exhibit topographical changes as detected by height imaging (*arrows*). These results demonstrate that initially Aβ fibrils may be accommodated within the lipid headgroups. (*C*) Aβ1–40 solution examined at 24 h fails to demonstrate the presence of Aβ fibrils, suggesting that fibrils are not formed in solution and subsequently associate with the bilayer. Scale bars, 200 nm.

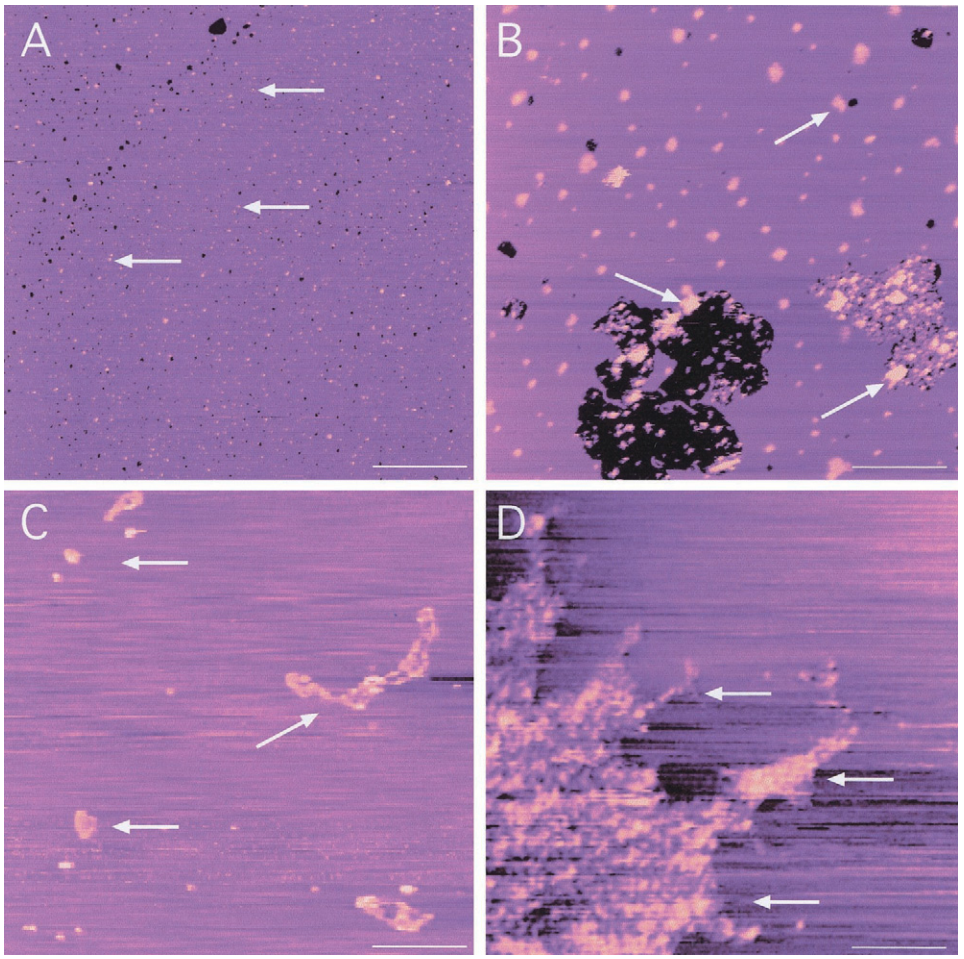

FIGURE 6 In situ TMAFM images acquired in PBS of the interaction of Aβ1–40 with DMPC bilayers. Intact DMPC bilayers are smooth, essentially defect free, before the addition of peptide. (*A*) In the presence of DMPC bilayers, the Aβ1−40 peptide partially inserts into the bilayer. (*B*) Extended duration in situ TMAFM reveals the gradual growth and lateral aggregation of Aβ1−40 within the DMPC bilayers, which results in minimal bilayer disruption. TMAFM images acquired in PBS of the interaction of preformed Aβ1–40 fibrils with total brain lipid extract bilayers. (*C*) After the addition of small preformed fibrils, Aβ can be detected above the surface of the bilayer in the absence of membrane disruptions. (*D*) Large aggregate Aβ masses can also be detected on intact bilayers, even after extensive incubation. Scale bars, 200 nm (*A* and *B*) and 100 nm (*C* and *D*).

formed by incubation of Aβ1−40 at 10 mg/ml for 3 days had the characteristic amyloid fibrillar structure (Fig. 2 *C*). To examine the effects of both protofibril and aggregates on the stability of the planar bilayers, we examined Aβ1−40 after short and long incubation periods. On total brain lipid extract bilayers, small preformed Aβ1–40 fibrils formed after short incubation were found on the bilayer surface but did not extend into, or disrupt, the bilayers (Fig. 6 *C*). The fibers detected by TMAFM extended 20–30 Å above the bilayer surface. Upon interaction with the bilayer, all fibrils appeared to circle back on themselves to form enclosed ring-type structures rather than the extended fibrils detected in the absence of lipid. These dimensions and fibril characteristics are similar to those previously examined by AFM in the presence of synthetic phosphatidylethanolamine and phosphatidylserine vesicles (Lin et al., 1999). Even after 24 h of incubation, both the Aβ fibrils and the bilayer remained intact. Additional incubation of these fibrils results in lateral aggregation into large Aβ masses in which individual fibers are not readily distinguishable. Addition of these aggregates onto the bilayer surface results in massive peptide aggregates extending 50–100 Å above the bilayer but does not result in bilayer disruption (Fig. 6 *D*). These results reinforce our proposal that self-assembly of Aβ on the surface of the bilayer is critical for membrane disruption.

Aβ sequence requirements for membrane disruption

To investigate the relationship between Aβ sequence and the extent of membrane insertion, we examined the propensity of Aβ1–28, the extracellular domain of Aβ, to induce membrane disruption. Aβ1–28 lacks the hydrophobic C-terminal domain of Aβ1–40 but still assembles into β-sheet fibrils, with the conversion between α-helix, random coil, and β-structure in Aβ1–28 being highly dependent on solution conditions (Barrow and Zagorski, 1991; Brooksbank and Marinez, 1989; Fletcher and Keire, 1997). TMAFM height and phase imaging revealed aggregation of Aβ1–28 on both total brain lipid and DMPC bilayers (Fig. 7). In both cases, extended duration TMAFM indicated that membrane destabilization resulted from lateral expansion of aggregated Aβ1–28 patches on the bilayer. DMPC bilayers formed within the AFM fluid cell demonstrate random membrane defects and a few lipid globules sitting on the

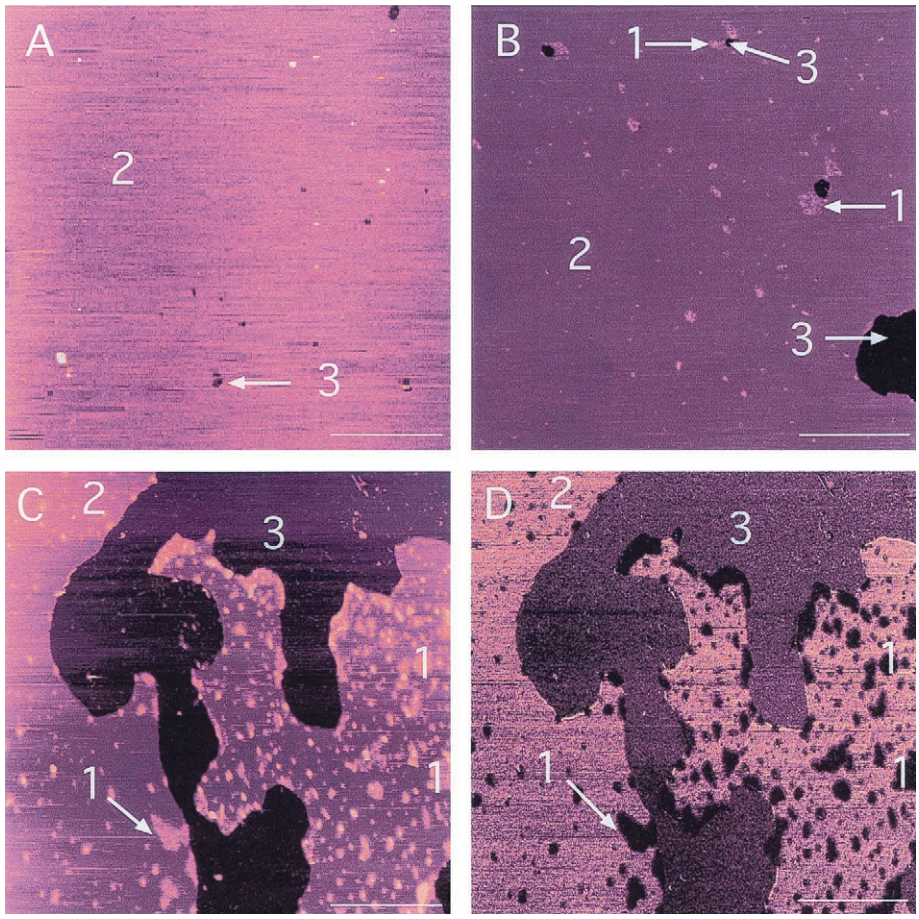

FIGURE 7 In situ TMAFM images acquired in PBS of the interaction between Aβ1–28 and DMPC bilayers. The initial DMPC bilayer was smooth with minimal bilayer defects (*A*). (*B*) Patches of Aβ1–28 peptide (*1*) can be seen aggregating on the surface of the DMPC bilayers (*2*) 30 min after introduction of the Aβ1–28 protein solution. (*C* and *D*) TMAFM height (*C*) and phase (*D*) images of the DMPC bilayers 15 h after introduction of Aβ1–28. The DMPC bilayer is extensively disrupted and large patches of Aβ1–28 (*1*) are evident on the surface of the remaining bilayer regions (*2*). The phase image shown in *D* provides definition of Aβ1–28 patches seen in *C*. Regions marked *3* denote the bare mica surface. (*A–D*) Scale bar, 800 nm. (*A–C*) Images are height encoded by color with the lower underlying mica shown in black. In this scheme, the lighter colored regions represent the 12–25-Å-thick Aβ1–28 patches residing on top of the 40-Å-thick bilayer. Superposition of the height and phase-contrast images revealed direct correspondence between the dark regions on the phase image, indicative of increased adhesion and energy dissipation, with the regions identified as Aβ1–28 aggregates on the lipid surface.

surface of the bilayer (Fig. 7 *A*). The lipid globules can be distinguished from peptide using both height and phase imaging. At initial time points, small aggregates of Aβ1–28 were associated with membrane holes of varying size or on the surface of the bilayer (Fig. 7 *B*). As in our results with the Aβ1–40 peptide, the absence of obvious aggregates on the exposed mica surface demonstrates that the peptide prefers to associate with the lipid bilayer. The amount of peptide associated with the bilayer could not be directly correlated with the size of the hole, although membrane defects did not form in the absence of peptide (Fig. 7 *C*). Similar results wherein the extent of membrane disruption cannot be directly correlated to the extent of the perturbation have been observed for other bilayer systems and been described as spinodal decomposition (Sackman and Feder, 1995; Tsai and Torkelson, 1989). Phase imaging confirmed the presence of Aβ peptide at the bilayer edges and demonstrated the association of Aβ with pre-existing Aβ aggregates, suggesting that Aβ-Aβ interactions increase with time (Fig. 7 *D*). Because membrane destabilization occurred in the complete absence of fibril formation, we propose that self-aggregation of Aβ at the lipid surface is sufficient to cause local disruptions in membrane integrity.

DISCUSSION

Our CD and in situ TMAFM investigations of Aβ-lipid interactions have revealed that Aβ membranolytic action depends on Aβ structure and lipid environment. Our observations by in situ TMAFM that suggests that Aβ1–40 undergoes partial insertion into lipid membranes contradicts previous x-ray diffraction and fluorescence data that reported complete Aβ1–40 insertion into the hydrocarbon region of the bilayer (Mason et al., 1996, 1999; Mirzabekov et al., 1994; Pillot et al., 1996). However, in contrast to our approach where monomeric Aβ1–40 was added to preformed lipid bilayers, these earlier studies were performed on lipid bilayers prepared in the presence of Aβ. Energetically, preparing lipid bilayers by the latter method favors burying the hydrophobic Aβ peptide within the lipid acyl chains to generate a stable bilayer structure. Moreover, because it is known that in vivo the Aβ peptide is released in a monomeric form, it is therefore appropriate to investigate how the freely soluble peptide will interact with membrane-mimetic surfaces under analogous conditions (Esch et al., 1990; Haass et al., 1992).

Previous studies have demonstrated that acidic phospholipids and phosphoinositides promote a conformational tran-

sition in Aβ from random to β-structure (Arispe et al., 1993; Choo-Smith and Surewicz, 1997; Mason et al., 1996; 1999; McLaurin and Chakrabartty, 1996, 1997; McLaurin et al., 1997, 1998; Mirzabekov et al., 1994; Pillot et al., 1996; Terzi et al., 1994, 1995). We now have evidence suggesting that this lipid-induced conformational transition is facilitated by Aβ's C-terminal hydrophobic domain. By forming a β-sheet scaffold structure, the sterically compact Aβ peptide can reside within or on the surface of the lipid headgroups and self-associate to form the critical fibril nucleus. After nucleation, fibril growth through the lipid bilayer ultimately results in destabilization of the membrane through excision of bilayer regions (Fig. 7). These results are in agreement with Kremer and colleagues (2000), who reported that Aβ-induced changes in membrane fluidity were dependent on insertion of Aβ into the fatty acyl chains of the bilayer. In the absence of acidic lipids or a C-terminal hydrophobic domain, Aβ fibril formation is abolished; however, membrane disruption still occurs via expansion of aggregated Aβ through the bilayer. Our observation that aggregation of the truncated Aβ1–28 peptide occurred on the total brain lipid and DMPC. Comparison of the lateral size and thickness of the aggregated Aβ1–28 patches on the total brain lipid bilayers with those found on the neutral DMPC bilayers demonstrate that patches on total brain lipid bilayers were smaller laterally but thicker than those found on the DMPC bilayers. We attribute these observations to preferential binding of Aβ1–28 to small, possibly acidic, lipid domains within the heterogeneous total brain lipid bilayers followed by Aβ1–28 self-association within these domains. Based on these observations, we propose that the steric bulk of randomly structured Aβ peptide cannot be readily accommodated by the lipid headgroups and gradual enlargement of the Aβ1–28 patches facilitates local disruption of the bilayers (Fig. 8).

Based on our observations, we propose the following two-stage model for the membranolytic action of Aβ. Assembly of Aβ leads to highly localized disruption of the membrane. This disruption may enable ions to pass freely between the intra- and extracellular space and is consistent with reports that Aβ enhances ion fluxes, thereby altering cellular homeostasis (Arispe et al., 1993; Mirzabekov et al., 1994). Increasing accumulation of Aβ and the initiation of fibril formation through the membrane results in destabilization of larger regions of the membrane. These openings may facilitate the passage of proteins, as has been demonstrated for endosomal-lysosomal vesicles, resulting in the protein compartmentalization errors characteristic of Alzheimer's disease (Avdulov et al., 1997; Blanc et al., 1997; Cataldo et al., 1996; Yang et al., 1998). The presence of cell

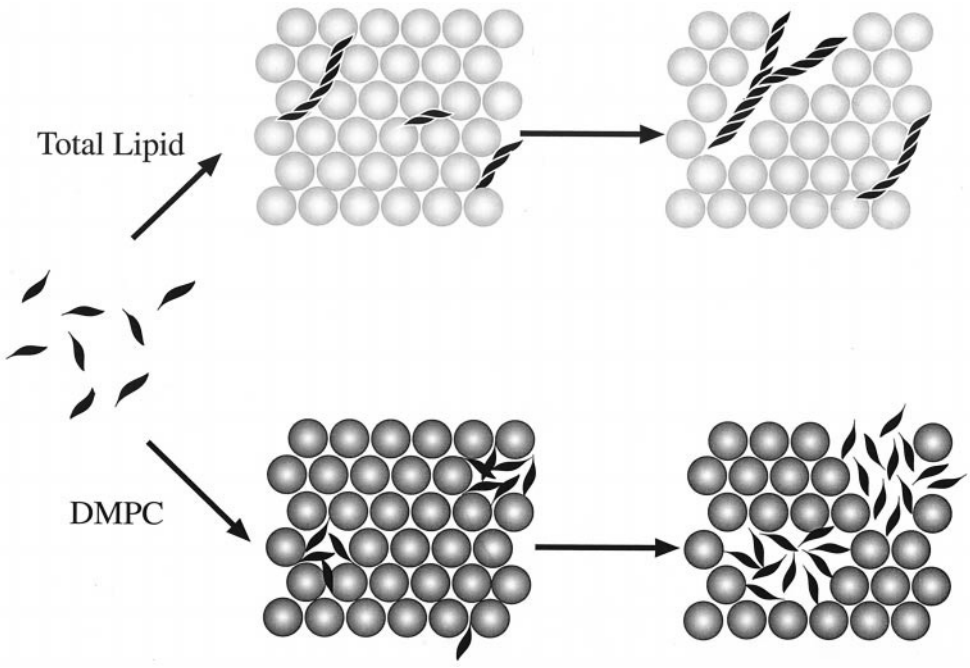

FIGURE 8 Schematic model of the interaction between Aβ peptides and lipid bilayers. Initial Aβ-lipid bilayer interaction, either through insertion of the hydrophobic domain or surface interaction with the lipid headgroups (peptide indicated in black), is readily accommodated. In the presence of acidic lipid, fibril formation occurs as a result of a lipid-induced structural transition (total lipid pathway). Fibril growth occurs through the bilayer resulting in displacement of lipid and eventual excision of large regions of the bilayer. In the absence of acidic lipid, fibril formation is abolished and Aβ aggregation occurs (DMPC pathway). This process leads to disruption of the lipid headgroups and localized destabilization of the bilayer. Small bilayer defects are formed adjacent to small Aβ aggregates. Growth of the Aβ aggregates is accompanied by an increasing localized bilayer disruption and lateral expansion of the bilayer defect.

surface fibril formation was eloquently demonstrated on cerebrovascular smooth muscle cells using EM (Van Nostrand et al., 1998), and plasma-membrane-bound Aβ is the initiation site for deposition of diffuse plaques (Yamaguchi et al., 2000). Finally, the inability of preformed Aβ fibrils to induce membrane disruption correlates well with the lack of in vitro toxicity observed when neuronal and cerebrovascular smooth muscle cells are incubated with preformed Aβ fibrils (Davis-Salinas and Van Nostrand, 1995; May et al., 1992). Recent studies detailing the importance of the C-terminal region of Aβ for its neurotoxic properties have demonstrated that nonfibrillar Aβ induces an apoptotic death in neurons whereas aggregated Aβ induces a necrotic death (Pillot et al., 1999). Our TMAFM studies have provided structural evidence of how these processes may take place and, in particular, how membrane disruption can be triggered by alternate structures of the same peptide. This and related approaches to studying protein assembly (or misassembly) at membrane interfaces will facilitate real-time investigations of the mechanisms by which specific protein-lipid interactions are driven by either sequence, structure, or compositional differences and will be of particular applicability for investigating other amyloidogenic pathways.

We thank Dr. N. Wang at the Hospital for Sick Children's Biotechnology Centre for the synthesis of all peptides used in this study, Dr. A. Chakrabartty for use of the Aviv Circular Dichroism Spectrometer, and the Electron Microscopy Suite at the University of Toronto for use of Hitachi 7000 electron microscope.

C.M.Y. gratefully acknowledges the generous support of the Medical Research Council of Canada (MT-14769), the Natural Sciences and Engineering Research Council of Canada (194435–99), the Ontario Research and Development Challenge Fund, and the University of Toronto's Connaught Foundation grant (413578). J.M. acknowledges support from the Kevin Burke Memorial Amyloid Fund (407966), the University of Toronto Dean's Fund (414744), the Banting Research Foundation (415961), and the Bickell Foundation (416157).-32767

REFERENCES

Arispe, N., E. Rojas, and H. B. Pollard. 1993. Alzheimer disease amyloid beta protein forms calcium channels in bilayer membranes: blockade by tromethamine and aluminum. *Proc. Natl. Acad. Sci. U.S.A.* 90:567–571.

Avdulov, N. A., S. V. Chochina, U. Igbavboa, E. O. O'Hare, F. Schroeder, J. P. Cleary, and W. G. Wood. 1997. Amyloid beta-peptides increase annular and bulk fluidity and induce lipid peroxidation in brain synaptic plasma membranes. *J. Neurochem.* 68:2086–2091.

Barrow, C. J., and M. G. Zagorski. 1991. Solution structures of beta peptide and its constituent fragments: relation to amyloid deposition. *Science.* 253:179–182.

Bayerl, T. M., and M. Bloom. 1991. Physcial properties of single phospholipid bilayers adsorbed to micro glass beads. A new vesicular model system studied by ^{2}H-nuclear magnetic resonance. *Biophys. J.* 58: 357–362.

Behl,, C., Davis, J. B., Klier, F. G., and Schubert, D. 1994. Amyloid beta peptide induces necrosis rather than apoptosis. *Brain Res.* 645:253–264.

Blackley, H. K. L., N. Patel, M. C. Vaies, C. J. Roberts, S. J. B. Tendler, M. J. Wilkinson, and P. M. Williams. 1999. Morphological development of beta(1–40) amyloid fibrils. *Exp. Neurol.* 158:437–443.

Blanc, E. M., M. Toborek, R. J. Mark, B. Hennig, and M. P. Mattson. 1997. Amyloid beta-peptide induces cell monolayer albumin permeability, impairs glucose transport, and induces apoptosis in vascular endothelial cells. *J. Neurochem.* 68:1870–1881.

Brandsch, R. G., G. Bar, and M-H. Whangbo. 1997. On the factors affecting the contrast of height and phase images in tapping mode atomic force microscopy. *Langmuir.* 13:6349–6353.

Brian, A. A., and H. M. McConnell. 1984. Allogenic stimulation of cytotoxic T cells by supported planar membranes. *Proc. Natl. Acad. Sci. U.S.A.* 81:6159–6163.

Brooksbank, B. W. L., and M. Marinez. 1989. Lipid abnormalities in the brain in adult Down's syndrome and Alzheimer's disease. *Mol. Chem. Neuropathol.* 15:157–185.

Cai, X.-D., T. E. Golde, and G. S. Younkin. 1993. Release of excess amyloid beta protein from a mutant amyloid beta protein precursor. *Science.* 259:514–516.

Cataldo, A. M., D. J. Hamilton, J. L. Barnett, P. A. Paskevich, and R. A. Nixon. 1996. Properties of the endosomal-lysosomal system in the human central nervous system: disturbances mark most neurons in populations at risk to degenerate in Alzheimer's disease. *J. Neurosci.* 16:186–199.

Choo-Smith, L.-P., and W. K. Surewicz. 1997. Acceleration of amyloid fibril formation by specific binding of Abeta-(1–40) peptide to ganglioside-containing membrane vesicles. *FEBS Lett.* 402:95–98.

Citron, M., C. Vigo-Pelfrey, D. B. Teplow, C. Miller, D. Schenk, J. Johnston, B. Winblad, N. Venizelos, L. Lannfelt, and D. Selkoe. 1994. Excessive production of amyloid beta-protein by peripheral cells of symptomatic and presymptomatic patients carrying the Swedish familial Alzheimer disease mutation. *Proc. Natl. Acad. Sci. U.S.A.* 91: 11993–11997.

Cleveland, J. P., B. Anczykowski, A. E. Schmid, and V. B. Elings. 1998. Energy dissipation in tapping-mode atomic force microscopy. *Appl. Phys. Lett.* 72:2613–2615.

Czajkowsky, D. M., M. J. Allen, V. Elings, and Z. F. Shao. 1998. Direct visualization of surface charge in aqueous solution. *Ultramicroscopy.* 74:1–5.

Davis-Salinas, J., and W. E. Van Nostrand. 1995. Amyloid beta-protein aggregation nullifies its pathologic properties in cultured cerebrovascular smooth muscle cells. *J. Biol. Chem.* 270:20887–20890.

Esch, F., P. S. Keim, E. C. Beattie, R. W. Blacher, and A. R. Culwell. 1990. Cleavage of amyloid beta peptide during constitutive processing of its precursor. *Science.* 248:1122–1128.

Fletcher, T. G., and D. A. Keire. 1997. The interaction of beta-amyloid protein fragment (12–28) with lipid environments. *Protein Sci.* 6:666–675.

Giulian, D., L. J. Haverkamp, J. H. Yu, W. Karshin, D. Tom, J. Li, J. Kirkpatrick, L. M. Luo, and A. E. Roher. 1996. The HHQK domain of β-amyloid provides a structural basis for the immunopathology of Alzheimer's disease. *J. Neurosci.* 16:6021–6037.

Groves, J. T., N. Ulman, and S. G. Boxer. 1997. Micropatterning fluid lipid bilayers on solid supports. *Science.* 275:651–653.

Haass, C., M. G. Schlossmacher, A. Y. Hung, C. Vigo-Pelfrey, A. Mellon, B. L. Ostaszewski, I. Lieberburg, E. H. Koo, D. Schenk, D. B. Teplow, and D. J. Selkoe. 1992. Amyloid beta-peptide is produced by cultured cells during normal metabolism. *Nature.* 359:322–325.

Halverson, K., P. E. Fraser, D. A. Kirschner, and P. T. Lansbury. 1990. Molecular determinants of amyloid deposition in Alzheimer's disease: conformational studies of synthetic beta-protein fragments. *Biochemistry.* 29:2639–2644.

Hansma, P. K., J. P. Cleveland, M. Radmacher, D. A. Walters, P. E. Hillner, M. Bezanilla, M. Fritz, D. Vie, H. G. Hansma, C. B. Prater, J. Massie, J. Gurley, and V. Elings. 1994. Tapping mode atomic-force microscopy in liquids. *Appl. Phys. Lett.* 64:1738–1740.

Harper, J. D., S. S. Wong, C. M. Lieber, and P. T. Lansbury. 1997. Atomic force microscopic imaging of seeded fibril formation and fibril branching by the Alzheimer's disease amyloid-b protein. *Chem. Biol.* 4:119–125.

Huang, T. H. J., D. S. Yang, N. P. Plaskos, S. Go, C. M. Yip, P. E. Fraser, and A. Chakrabartty. 2000. Structural studies of soluble oligomers of the Alzheimer beta-amyloid peptide. *J. Mol. Biol.* 297:73–87.

Iwatsubo, T., D. Mann, A. Odaka, N. Suzuki, and Y. Ihara. 1995. Amyloid beta protein (Abeta) deposition: Abeta 42(43) precedes Abeta 40 in Down syndrome. *Ann. Neurol.* 37:294–299.

Jao, S.-C., K. Ma, J. Talafous, R. Orlando, and M. G. Zagorski. 1997. Trifluoroacetic acid pretreatment reproducibly disaggregates the amyloid beta-peptide. *Amyloid Int. J. Exp. Clin. Invest.* 4:240–252.

Karrasch, S., R. Hegerl, J. Hoh, W. Baumeister, and A. Engel. 1994. Scanning force microscopy produces faithful high resolution images of protein surfaces in an aqueous environment. *Proc. Natl. Acad. Sci. U.S.A.* 91:836–838.

Kirschner, D. A., C. Abraham, and D. J. Selkoe. 1986. X-ray diffraction from intraneuronal paired helical filaments and extraneuronal amyloid fibers in Alzheimer's disease indicates cross-β conformation. *Proc. Natl. Acad. Sci. U.S.A.* 83:503–507.

Kowalewski, T., and D. M. Holtzman. 1999. In situ atomic force microscopy study of Alzheimer's beta-amyloid peptide on different substrates: new insights into mechanism of beta-sheet formation. *Proc. Natl. Acad. Sci. U.S.A.* 96:3688–3693.

Kremer, J. J., M. M. Pallitto, D. J. Sklansky, and R. M. Murphy. 2000. Correlation of β-amyloid aggregate size and hydrophobicity with decreased bilayer fluidity of model membranes. *Biochemistry.* 39: 10309–10318.

Lin, H., Y. J. Zhu, and R. Lal. 1999. Amyloid beta protein (1–40) forms calcium-permeable, Zn^{2+} sensitive channel in reconstituted lipid vesicles. *Biochemistry.* 38:11189–11196.

Lomakin, A., D. S. Chung, G. B. Benedek, D. A. Kirschner, and D. B. Teplow. 1996. On the nucleation and growth of amyloid beta-protein fibrils: detection of nuclei and quantitation of rate constants. *Proc. Natl. Acad. Sci. U.S.A.* 93:1125–1129.

Lorenzo, A., and B. Yankner. 1994. Beta-amyloid neurotoxicity requires fibril formation and is inhibited by Congo red. *Proc. Natl. Acad. Sci. U.S.A.* 91:12243–12247.

Marquess, S., V. H. Robbins, and R. L. Baldwin. 1989. Unusually stable helix formation in short alanine-based peptides. *Proc. Natl. Acad. Sci. U.S.A.* 86:5286–5290.

Mason, R. P., J. D. Estermeyer, J. F. Kelly, and P. E. Mason. 1996. Alzheimer's disease amyloid beta peptide 25–35 is localized in the membrane hydrocarbon core: x-ray diffraction analysis. *Biochem. Biophys. Res. Commun.* 222:78–82.

Mason, R. P., R. F. Jacob, M. F. Walter, P. E. Mason, N. A. Avdulov, S. V. Chochina, U. Igbavboa, and W. G. Wood. 1999. Distribution and fluidizing action of soluble and aggregated amyloid beta-peptide in rat synaptic plasma membranes. *J. Biol. Chem.* 274:18801–18807.

Masters, C. L., G. Simms, N. A. Weinman, G. Multhaup, B. L. McDonald, and K. Beyreuther. 1985. Amyloid plaque core protein in Alzheimer disease and Down syndrome. *Proc. Natl. Acad. Sci. U.S.A.* 82: 4245–4249.

Mattson, M. A., J. G. Begley, R. J. Mark, and K. Furukawa. 1997. Aβ25–35 induces rapid lysis of red blood cells: contrast with Aβ1- 42 and examination of underlying mechanisms. *Brain Res.* 771:147–153.

May, P. C., B. D. Gitter, D. C. Waters, L. K. Simmons, G. W. Becker, J. S. Small, and P. M. Robinson. 1992. β-Amyloid peptide in vitro toxicity: lot-to-lot variability. *Neurobiol. Aging.* 13:605–607.

McLaurin, J., and A. Chakrabartty. 1996. Membrane disruption by Alzheimer β-amyloid peptides mediated through specific binding to either phospholipids or gangliosides. Implications for neurotoxicity. *J. Biol. Chem.* 271:26482–26489.

McLaurin, J., and A. Chakrabartty. 1997. Characterization of the interactions of Alzheimer β-amyloid peptides with phospholipid membranes. *Eur. J. Biochem.* 245:355–363.

McLaurin, J., T. Franklin, P. E. Fraser, and A. Chakrabartty. 1997. Structural transitions associated with the interaction of Alzheimer β-amyloid peptides with gangliosides. *J. Biol. Chem.* 273:4506–4515.

McLaurin, J., D-S. Yang, C. M. Yip, and P. E. Fraser. 2000. Modulating factors in amyloid-β fibril formation. *J. Struct. Biol.* 130:259–270.

Mirzabekov, T., M.-C. Lin, W.-L. Yuan, D. J. Marshall, M. Carman, K. Tomaselli, I. Leiberburg, and B. L. Kagan.1994. Channel formation in planar lipid bilayers by a neurotoxic fragment of the β-amyloid peptide. *Biochem. Biophys. Res. Commun.*1142–1148.

Möller, C., M. Allen, V. Elings, A. Engel, and D. J. Müller. 1999. Tapping-mode atomic force microscopy produces faithful high-resolution images of protein surfaces. *Biophys. J.* 77:1150–1158.

Noy, A. C., H. Sanders, D. V. Vezenov, S. S. Wong, and C. M. Lieber. 1998. Chemically-sensitive imaging in tapping mode by chemical force microscopy: relationship between phase lag and adhesion. *Langmuir.* 14:1508–1511.

Oda, T., P. Wals, H. H. Soterburg, S. A. Johnson, G. M. Pasinetti, T. E. Morgan, I. Rozovsky, W. B. Stine, S. W. Snyder, and T. F. Holzman. 1995. Clusterin (apoJ) alters the aggregation of amyloid β-peptide ($A\beta_{1-42}$) and forms slowly sedimenting Aβ complexes that cause oxidative stress. *Exp. Neurol.* 136:22–31.

Paradis, E., H. Douillard, M. Koutroumanis, C. Goodyer, and A. LeBlanc. 1996. Amyloid beta peptide of Alzheimer's disease downregulates Bcl-2 and upregulates bax expression in human neurons. *J. Neurosci.* 16: 7533–7539.

Pike, C. J., D. Burdick, A. J. Walencewicz, C. G. Glabe, and C. W. Cotman. 1993. Neurodegeneration induced by β-amyloid peptides in vitro: the role of peptide assembly state. *J. Neurosci.* 13:1676–1687.

Pillot, T., B. Drouet, S. Queille, C. Labeur, J. Vandkerckhove, M. Rosseneu, M. Pincon-Raymond, and J. Chambaz. 1999. The nonfibrillar amyloid β-peptide induces apoptotic neuronal cell death: involvement of its C-terminal fusogenic domain. *J. Neurochem.* 73:1626–1634.

Pillot, T., M. Goethals, B. Vanloo, C. Talussot, R. Brasseur, J. Vandekerckhove, M. Rosseneu, and L. Lin. 1996. Fusogenic properties of the C-terminal domain of the Alzheimer β-amyloid peptide *J. Biol. Chem.* 271:28757–28765.

Plaskos, N. P., and C. M. Yip. 2000. Studies of biomolecular assemblies: in situ atomic force microscopy of inosine 5′-monophosphate dehydrogenase. *Biophys. J.* 78:292A.

Roher, A. E., M. O. Chaney, Y-M. Kuo, S. D. Webster, W. B. Stine, L. J. Haverkamp, A. S. Woods, R. J. Cotter, J. M. Tuohy, G. A. Krafft, B. S. Bonnell, and M. R. Emmerling. 1996. Morphology and toxicity of Aβ-(1–42) dimer derived from neuritic and vascular amyloid deposits of Alzheimer's disease. *J. Biol. Chem.* 271:20631–20635.

Roher, A., K. C. Palmer, E. C. Yurewics, M. J. Ball, and B. D. Greenberg. 1993. Morphological and biochemical analyses of amyloid plaque core proteins purified from Alzheimer disease brain tissue. *J. Neurochem.* 61:1916–1926.

Roher, A., D. Wolfe, M. Palutke, and D. KuKuruga. 1986. Purification, ultrastructure, and chemical analysis of Alzheimer disease amyloid plaque core protein. *Proc. Natl. Acad. Sci. U.S.A.* 83:2662–2666.

Sackman, E., and T. Feder. 1995. Budding, fission and domain formation in mixed lipid vesicles induced by lateral phase separation and macromolecular condensation. *Mol. Membr. Biol.* 12:21–28.

Salafsky, J., J. T. Groves, and S. G. Boxer. 1996. Architecture and function of membrane proteins in planar supported bilayers: a study with photosynthetic reaction centres. *Biochemistry.* 35:14773–14781.

Simmons, L. K., P. C. May, K. J. Tomaselli, R. E. Rydel, K. S. Fuson, E. F. Brigham, S. Wright, I. Lieberburg, G. W. Becker, D. N. Brems, and W. Y. Li. 1993. Secondary structure of amyloid β peptide correlates with neurotoxic activity in vitro. *Mol. Pharmacol.* 45:373–379.

Soto, C., E. M. Castano, A. Kumar, R. C. Beavis, and B. Frangione. 2000. 1995. Fibrillogenesis of synthetic amyloid-β peptides is dependent on their initial secondary structure. *Neurosci. Lett.*105–108.

Sticht, H., P. Bayer, D. Willbold, S. Dames, C. Hilbich, K. Beyreuther, R. W. Frank, and P. Rosch. 1995. Structure of amyloid Aβ-(1–40)-peptide of Alzheimer's disease. *Eur. J. Biochem.* 233:293–298.

Stine, W. B., Jr., S. W. Snyder, U. S. Ladror, W. S. Wade, M. F. Miller, T. J. Perum, T. F. Holzman, and G. A. Krafft. 1996. The nanometer-scale structure of amyloid-β visualized by atomic force microscopy. *J. Protein Chem.* 15:193–203.

Suzuki, N., T. T. Cheung, X. D. Cai, A. Odaka, L. Otvos, Jr., C. Eckman, T. E. Golde, and S. G. Younkin. 1994. An increased percentage of long

amyloid beta protein secreted by familial amyloid beta protein precursor (beta APP717) mutants. *Science.* 264:1336–1340.

Talafous, J., K. J. Marcinowski, G. Klopman, and M. G. Zagorski. 1994. Solution structure of residues 1–28 of the amyloid β-peptide. *Biochemistry.* 337788–7796.

Terzi, E., G. Holzemann, and J. Seelig. 1994. Alzheimer β-amyloid peptide 25–35: electrostatic interactions with phospholipid membranes. *Biochemistry.* 33:7434–7441.

Terzi, E., G. Holzemann, and J. Seelig. 1995. Self-association of β-amyloid peptide (1–40) in solution and binding to lipid membranes. *J. Mol. Biol.* 252:633–642.

Tsai, F. J., and J. M. Torkelson. 1989. On studying asymmetric membranes made from polymethylmethacrylate/xylene by the thermal-inversion method. *Prog. Clin. Biol. Res.* 292:119–128.

Van Nostrand, W. E., J. P. Melchor, and L. Ruffini. 1998. Pathologic amyloid beta-protein cell surface fibril assembly on cultured human cerebrovascular smooth muscle cells. *J. Neurochem.* 70:216–223.

Walsh, D. M., A. Lomakin, G. B. Benedek, M. M. Comdron, and D. B. Teplow. 1997. Amyloid beta-protein fibrillogenesis. Detection of a protofibrillar intermediate. *J. Biol. Chem.* 272:22364–22372.

Winkler, R. G., J. P. Spatz, S. Sheiko, M. Moller, P. Reineker, and O. Marti. 1996. Imaging material properties by resonant tapping-force microscopy: a model investigation. *Phys. Rev. B.* 54:8908–8912.

Yamaguchi, H., M. L. C. Maat-Schieman, S. G. van Duinen, F. A. Prins, P. Neeskens, R. Natte, and R. A. C. Roos. 2000. Amyloid β protein (Aβ) starts to deposit as plasma membrane-bound form in diffuse plaques of brains from hereditary cerebral hemorrhage with amyloidosis-Dutch type, Alzheimer disease and nondemented aged subjects. *J. Neuropathol. Exp. Neurol.* 59:723–732.

Yang, A. J., D. Chandswangbhuvana, L. Margol, and C. G. Glabe. 1998. Loss of endosomal/lysosomal membrane impermeability is an early event in amyloid Aβ1–42 pathogenesis. *J. Neurosci. Res.* 52:691–698.

Yang, J. T., C-S. C. Wu, and H. M. Martinez. 1986. Calculation of protein conformation from circular dichroism. *Methods Enzymol.* 130:208–269.

Yang, D.-S., C. M. Yip, T. H. J. Huang, A. Chakrabartty, and P. E. Fraser. 1999. Manipulating the amyloid-β aggregation pathway with chemical chaperones. *J. Biol. Chem.* 274:32970–32974.

Yip, C. M., M. L. Brader, B. H. Frank, M. R. DeFelippis, and M. D. Ward. 2000. Structural studies of a crystalline insulin analog complex with protamine by atomic force microscopy. *Biophys. J.* 78:466–473.

Yip, C. M., M. L. Brader, M. D. Ward, and M. R. DeFelippis.1998a. Atomic force microscopy of crystalline insulins: The influence of sequence variation on crystallization and interfacial structure. *Biophys. J.* 74:2199–2209.

Yip, C. M., M. R. DeFelippis, B. H. Frank, M. D. Ward, and M. L. Brader. 1998b. Structural and morphological characterization of ultralente insulin crystals by atomic force microscopy: evidence of hydrophobically driven assembly. *Biophys. J.* 74:1172–1179.

Yip, C. M., and M. D. Ward. 1996. Atomic force microscopy of insulin single crystals: direct visualization of molecules and crystal growth. *Biophys. J.* 71:1071–1078.